Chemical Methodologies 8(2024) 133-153

Chemical Methodologies

Journal homepage: http://chemmethod.com

Original Article

Biodiesel Production from Waste Cooking Oil Using Two-Dimensional Photocatalysts: Optimization of Process, Mechanism and Kinetics Study

Zahra Abbasi[1], Elisa I. Garcia-Lopez[2], Giuseppe Marci[3], Mehdi Ahmadi[4, 5*]

[1]*Faculty of Science, Ayatollah Boroujerdi University, Lorestan, Iran*
[2]*Department of Biological, Chemical and Pharmaceutical Sciences and Technologies (STEBICEF), University of Palermo, Viale delle Scienze, 90128 Palermo, Italy*
[3]*"Schiavello-Grillone" Photocatalysis Group, Department of Engineering, University of Palermo, Viale delle Scienze, 90128 Palermo, Italy*
[4]*Environmental Technologies Research Center, Ahvaz Jundishapur University of Medical Sciences, Ahvaz, Iran*
[5]*Department of Environmental Health Engineering, Ahvaz Jundishapur University of Medical Sciences, Ahvaz, Iran*

ARTICLEINFO

Article history
Submitted: 2023-12-08
Revised: 2024-01-12
Accepted: 2024-02-01
Manuscript ID: CHEMM-2312-1743
Checked for Plagiarism: Yes
Language Checked: Yes

DOI:10.48309/CHEMM.2024.429360.1743

KEYWORDS
Biodiesel
Two dimensional
Photocatalyst
Waste oil
Kinetics
Esterification

ABSTRACT

Biodiesel fuel is an alternative to diesel fuel. Burning biodiesel results in less pollution because its source is vegetable or animal fat. In this study, waste cooking oil (WCO) was used as raw material in the production of biodiesel. The content of free fatty acids (FFAs) in the studied WCO was 4.09%. Production of biodiesel from waste cooking oil was performed by a two-step method. In the first step, under visible irradiation, Cr (x%)-TiO_2 photocatalytic esterification of methanol with FFAs in WCO was studied. In the second step, NaOH catalyzed the transesterification of triglycerides with methanol. It was observed that in the presence of TiO_2, the efficiency rose by %10 compared with the case without photocatalysts. The order of photo-esterification reaction by Cr-TiO_2 was equal to 1. The activation energy required for the Cr-TiO_2 photocatalyst to photo-esterification WCO was 31.36 kJ/mol, confirming the realization of the reaction in mild conditions. Concerning the production of H^+, $CH_3OO^\cdot$ and R-COOH on the photocatalyst surface, we proposed a possible reaction mechanism for the esterification process. The mechanism of the transesterification reaction, OH^- was considered as the active species. According to the obtained results, the generated biodiesel density was 0.89 $g.cm^{-3}$. The pour point and the cloud point for biodiesel are obtained as -5 and 0, respectively. The viscosity of 4.1 $mm^2.s^{-1}$ biodiesel from waste oil was measured, which corresponded to the standard range. The acid value of the biodiesel sample obtained from the waste oil is 0.38 mg KOH g^{-1}.

* Corresponding author: Mehdi Ahmadi
E-mail: Ahmadi241@gmail.com

GRAPHICAL ABSTRACT

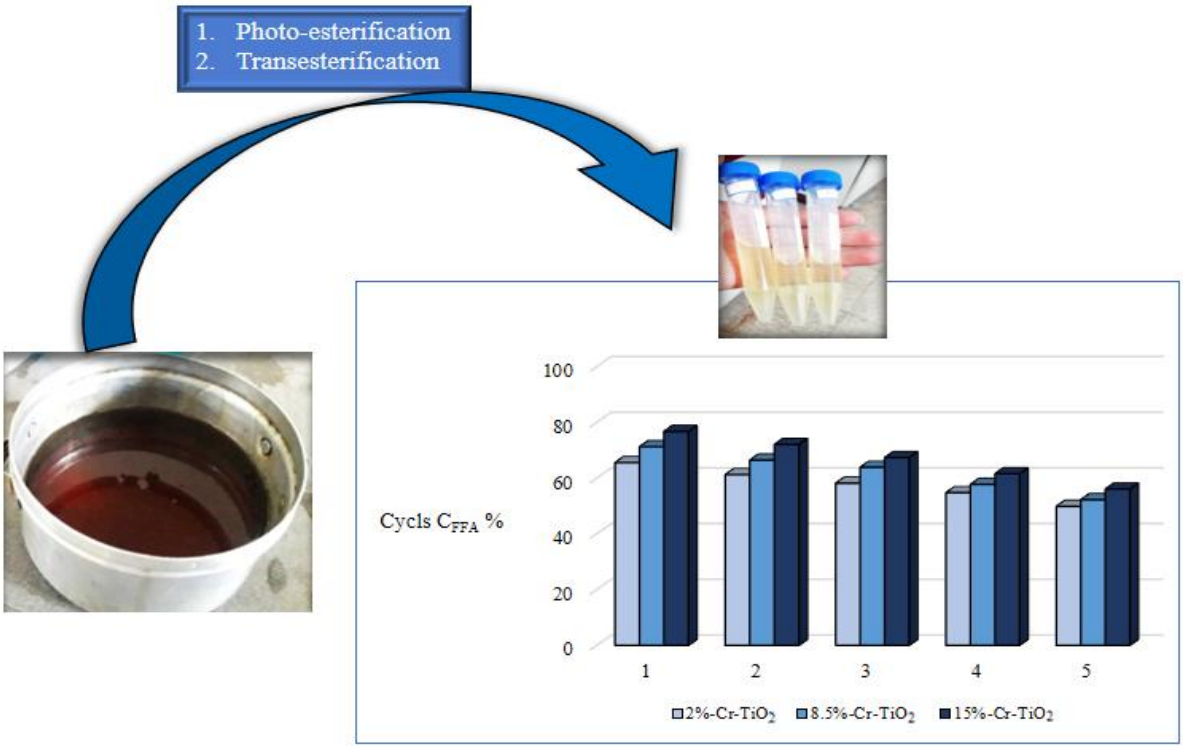

Introduction

Biofuels such as biodiesel are obtained from edible, non-edible plants, animal fats, waste oils, etc. According to the standards, biodiesel is the combination of long-chain mono alkyl esters of fatty acids resulting from the reaction of an alcohol with renewable lipid materials [1,2]. Biodiesel is produced from a variety of vegetable oil sources such as soybean, sunflower, cottonseed, etc. [3-7]. However, the future of the use of these edible oils is uncertain due to the increasing global food demand. In addition, the use of edible oils for biodiesel significantly increases its production costs [8-10]. The use of edible oil waste is a cost-effective way to produce fuel from waste materials. For the biodiesel synthesis from edible and non-edible oils, in addition to enzymes, two types of homogeneous or heterogeneous acidic and basic catalysts have been used. Homogeneous catalysts are difficult to recover and lead to waste generation. Today, the use of heterogeneous catalysts has become more common so that the catalyst can be easily recovered after biodiesel production. The most common method for biodiesel synthesis is through the transesterification reaction, in which a catalytic chemical reaction including vegetable oil and alcohol is used to produce fatty acid alkyl esters (biodiesel) and glycerol [11-13]. The morphology of a heterogeneous catalyst is one factor affecting its activity [14-16]. Due to the different morphology of a heterogeneous product, the amount of its optical, electronic, and catalytic properties varies. Many efforts have been made to improve the performance of titanium dioxide nanowires and nanostructures by making controlled size or shape at the nanoscale to improve photocatalytic, photovoltaic, electrochemical, and dielectric properties [17-21]. Statistical design for experimental experiments is considered a basic principle in conducting laboratory and industrial research. These designs achieve more reliable results, save time, significantly reduce the number of tests and ultimately lead to process optimization. The use of this method has been considered in laboratory works [22-24]. Recent studies have shown that a heterogeneous photocatalytic process may be performed to

efficiently esterification fatty acids without the problems of having a homogeneous catalyst. The first study was conducted by Corro *et al.* (2013) [25]. They used ZnO/SiO_2 photocatalyst to esterify the FFAs in Jatropha curcas crude oil, with fatty acid content above eighteen. In this study, the nanostructure of the photocatalyst in the photo-stratification stage has been used. The effect of the photo-esterification stage on the efficiency of biodiesel production from WCO has been investigated. Mengli *et al.* synthesized a highly active and reusable photocatalyst $La^{3+}/ZnO\text{-}TiO_2$ by sol-gel method [26].

Young-Moo *et al.* (2010) examined the esterification FFAs of vegetable oils using the heterogeneous WO_3/ZrO_2 catalyst. Values of 10-30% of WO_3 on ZrO_2 levels were investigated. It was observed that in the presence of 10, 20, and 30% of WO_3 showed 78%, 93%, and 89% efficiency, respectively. The effect of temperature on the reaction efficiency was investigated where in 2 h of reaction with increasing temperature from 75 °C to 200 °C, the conversion efficiency increased from 93% to 98% [27]. Also, Mazzocchia *et al.* (2004) studied the transesterification of triglycerides to fatty acid methyl esters in the presence of a heterogeneous catalyst using microwaves. They observed that the microwave method significantly reduced the reaction time [28].

Lertsathapornsuk *et al.* (2005) delved into the production of biodiesel from three types of coconut oil, rice husk, and palm oil. They used 800 W of microwave power and achieved the highest conversion rate in 1% sodium hydroxide as a catalyst and a molar ratio of alcohol to oil of 1 to 9 in 30 seconds. In 30 seconds, the conversion rates of 100%, 94% and 83% were obtained for coconut oil, rice husk and palm, respectively [29]. Likewise, Corro *et al.* (2017) reported the production of biodiesel from waste frying oil by a two-step process. In the first step, the FFAs in the oil were esterified using a photocatalytic process using a Cr/SiO_2 composite and solar radiation as a light source. The second step in the transesterification of triglycerides with methanol was performed by thermal activation using solar radiation as a light source and by NaOH. It was shown that the biodiesel obtained in this process possessed all the international requirements for use as fuel [30]. Abbasi and Ahmadi (2023) employed UV irradiation to decrease the free fatty acids (FFAs) of waste cooking oil (WCO). They showed Solid catalysts were found to be highly active for the photo-esterification of FFAs with methanol in the UV irradiation. While performing the esterification step in the presence of the UV irradiation in the presence of Cr-TiO2 photocatalysts, the efficiency was 76.3%-89.5% [31].

In this study, the percentage of FFAs in the oil was reduced by two-dimensional photocatalysts of titanium dioxide and titanium dioxide by doping chromium with different percentages. Three parameters were considered, including the amount of photocatalyst Cr (%2)-TiO_2, Cr (%8.5) -TiO_2 and Cr(%15)-TiO_2), the molar ratio of methanol to WCO (6 to 1, 9 to 1, and 12 to 1) and irradiation time (1 to 3 h) with the Box-Behnken mode to find the optimal points and maximum efficiency, followed by the analysis of variance. The optimal parameters to obtain the maximum production of biofuel were calculated. Relying on Verma method [32], we performed the transesterification step. The proposed kinetics and reaction mechanism for biodiesel production were scrutinized.

Materials and Methods

Waste Cooking Oil

In this study, the WCO was collected from restaurants and fast foods in the Lashkar Abad in Ahvaz, Iran. The WCO collected from restaurants contained water and solid particles, so it was initially separated using an impurity filter and fine solid particles. One of the factors that slow down the reaction process and reduce efficiency is the presence of water in the oil, which has a significant effect on the conversion percentage and quality of biodiesel produced. To remove the water in the waste oil, it was heated at 100 °C for three hours using continuous stirring to evaporate the water in the WCO.

Synthesis of 2D Cr-Doped-Tio₂

Cr-doped-TiO_2 nanoparticles were prepared using the hydrothermal method [33]. Titanium n-butoxide and chromium (III) acetylacetone were used as sources of Ti and Cr, respectively. Thus, 4.65 ml of titanium n-butoxide was dissolved in 45 ml of ethanol under stirring, and then 1.9 ml of hydrochloric acid was slowly added to the solution. Different concentrations of Cr were added to the resulting solution by adding chromium (III) acetylacetone for TiO_2 doping. The weight ratio of Cr to Ti in the synthesized catalyst was %2, %8.5 and %15, respectively, according to the Box-Behnken model design prediction. These photocatalysts are named: Cr (%2)-TiO_2, Cr (%8.5)-TiO_2 and Cr (%15)-TiO_2, respectively. After preparing the homogeneous solution for one day under stirring, the uniform solution was transferred to an autoclave and heated at 150 °C for 9 h.

After cooling to ambient temperature, the precipitates were separated by centrifugation and washed with large amounts of ethanol. Two-dimensional pure TiO_2 nanomaterials, doped with Cr, were calcined at 400 ° C for 1 h.

Steps To Perform the Reaction

A two-step schematic of biodiesel production, with WCO as the starting material, is displayed in Figure 1.

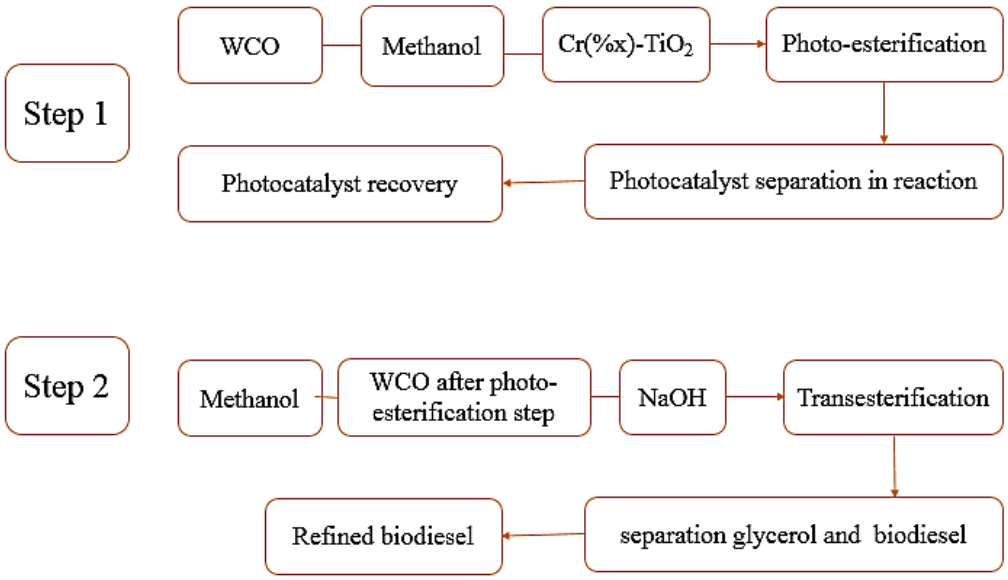

Figure 1: Two-step schematic of biodiesel production

Step 1: Photo-Esterification of Free Fatty Acid with Photocatalyst

The WCO obtained from the restaurant was used after removing the solids using a strainer and removing the water in the oil during the esterification step. A reactor equipped with a visible source was used to perform photo-esterification reactions. The device consists of two separate sections in the upper compartment that includes a mercury lamp 400 W and a cooler to reduce the temperature of the lamp and the lower compartment is placed to place the test sample.

The connection of the two chambers is made using a slit that uses a filter to remove wavelengths other than the wavelength in the visible light region. The experiment was set at ambient temperature and a stirring speed of 400 rpm. Figure 2 depicts a schematic of the photoreactor used in the study.

To consider ratios of methanol to oil, irradiation time and type of photocatalyst, a Box-Behnken design was used. FFA was esterified with methanol and 7.5wt% Cr(%x)-TiO_2 photocatalysts relative to oil in the above devices [8]. After esterification, the photocatalyst was

initially filtered and separated, and the excess methanol was recovered by distillation, and then the water was removed from the reaction solution by heating in an oven to prepare the esterified WCO for the second stage of transesterification. The optimization of reaction conditions and calculation of esterification rate under different reaction conditions were realized by Design-Expert software and Box- Behnken design method.

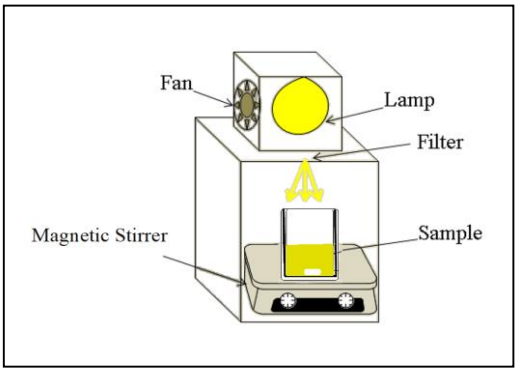

Figure 2: Schematic of the used reactor

The FFA% conversion rate was determined according to the acid content ratio using Equation (1):

$$\%C_{FFA} = \frac{A_i - A_t}{A_i} \times 100\% \quad (1)$$

Where, A_i is the initial acidic index of the waste cooking oil and A_t is the acidic index after the photo-esterification reaction.

Step 2: Transesterification

The transesterification reaction was performed according to the method of Verma *et al.* [32]. 32.5 g of esterified WCO was weighed, and then a molar ratio of methanol to oil of 6: 1 and 1.0 wt.% of NaOH was added to the flask and transferred to a two-portion balloon connected to a reflux refrigerant. The reactants were thoroughly mixed using a magnetic stirrer and a thermal oil bath was used to react at 60 °C. Reflux was performed for two hours. The yield of FAME was obtained by Equation (2):

$$\text{FAME } \% = \frac{\sum A - A_{IS}}{A_{IS}} \times \frac{C_{IS} \times V_{IS}}{m} \times 100 \quad (2)$$

Where, $\sum A$ is the sum of signal areas of fatty acid methyl esters (C14:0-C24:1), A_{IS} signifies the signal area of methyl heptadecanoate, C_{IS} symbolizes the concentration of methyl heptadecanoate, V_{IS} stands for the volume of standard solution, and m is the amount (mass) of biodiesel sample.

Photocatalyst Recovery and Reuse In The Photo-Esterification Process

Photocatalyst stability and its activity in reuse without significant reduction inefficiency is an important factor in heterogeneous photocatalytic processes. The reuse of catalysts is an important factor in evaluating the performance of a heterogeneous catalyst. In order to evaluate the stability of the photocatalyst, in the optimal conditions obtained with the software, five photo-esterification reactions were considered with Cr(%x)-TiO_2 catalysts with three percent different from Cr, and then biodiesel production with base catalyst was performed to confirm the recyclability of the photocatalyst.

After each experiment, two-dimensional pure Cr-doped TiO_2 nanomaterials were separated by centrifugation and filtration. It was then washed several times with ethanol, dried at 100 °C for 2 hours, and finally calcined for one hour at 400 °C for a repeatability test.

Results

Characterization of Photocatalyst

The surface morphology of the samples synthesized by the FESEM and TEM methods were investigated. The Figures show that the morphology of the samples is square and rectangular cubic titanium dioxide and have relatively identical dimensions. The images in Figures 3 demonstrate the layered structure of titanium dioxide with chromium particles scattered in the layers, causing the accumulation of sheets of titanium dioxide with chromium and the formation of an uneven surface of titanium dioxide. For a more detailed examination of these particles and their size at the nanometer scale, the following electron microscopic images are examined.

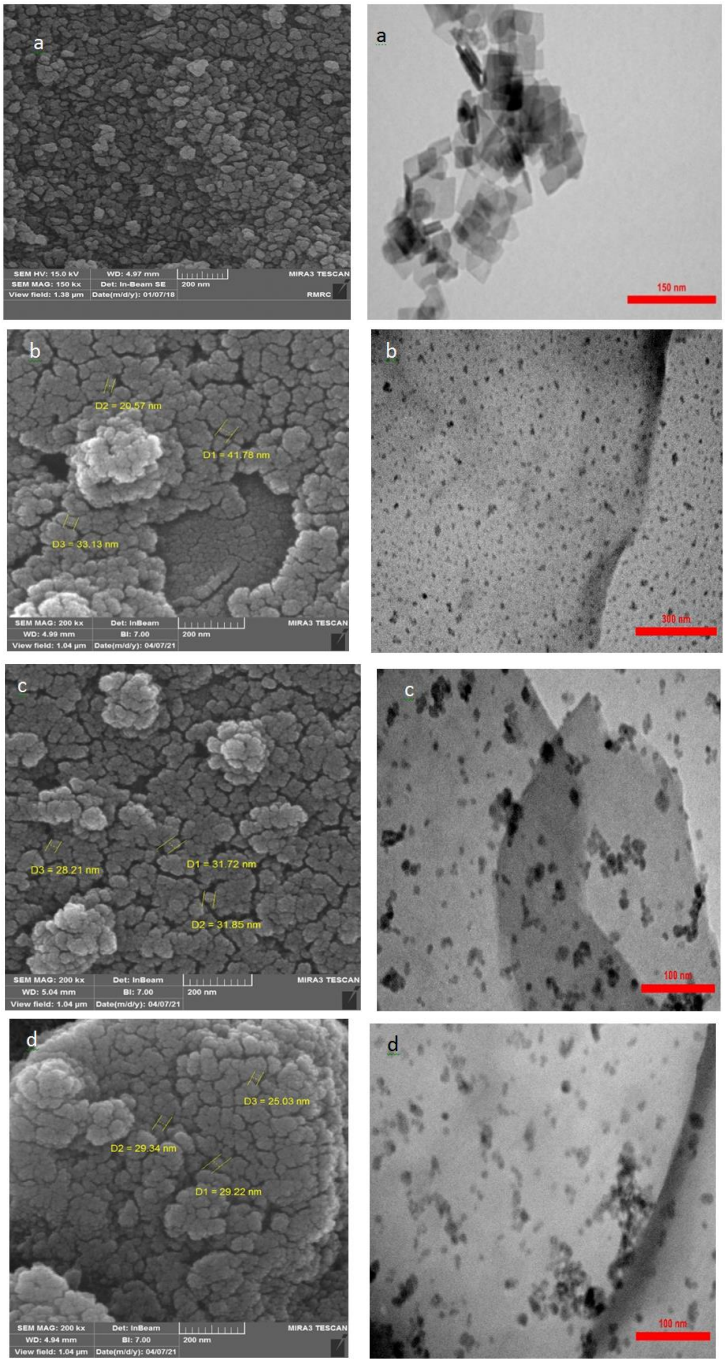

Figure 3: The FESEM and TEM images of a) pure TiO_2 b) Cr (%2)-TiO_2 c) Cr (%8.5)-TiO_2 and d) Cr (%15)-TiO_2

The morphology of the synthesized sample of titanium dioxide can be seen in two dimensions and in a square layer. In composite images of titanium dioxide with chromium particles, chromium particles are scattered on the surface of the titanium dioxide sheets. With an increasing percentage of chromium, the accumulation of these particles was observed on the surface of the titanium dioxide sheets.

The XRD patterns are illustrated in Figure 4. The characteristic diffraction peaks for the titanium dioxide of 2θ= 62.8°, 53.7°, 48.9°, 37.8°, and 25.1° relate to the anatase phase. This result is consistent with the structure of the titanium dioxide layers obtained in the report by Han *et al.* [33]. In the final composite pattern, all samples were synthesized in the anatase phase. Peaks 25.3°, 36.9°, 37.81°, 38.61°, 48.7°, 53.9, and 55.1° can be indexed to (101), (103), (004), (112), (200), (105), and (211) crystallographic planes of the anatase phase.

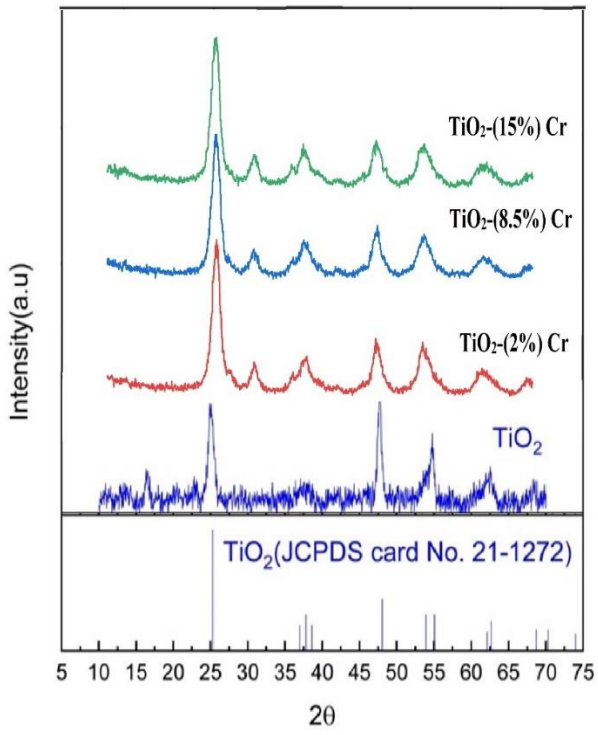

Figure 4: XRD patterns of nanocomposites

In the FT-IR spectra (Figure 5), in all synthesized samples, a broad absorption of 3400-3300 cm^{-1} is observed, which is related to the tensile vibration of the O-H bond present in the samples. The peaks in the 1740 and 1300 cm^{-1} regions are characterized by different states to the tensile vibrations of the Ti-O bond. Vibration peaks in the range of 700-400 cm^{-1} confirm the presence of Ti-O groups in the crystalline form of anatase in these nanocomposites, which is the result of tensile vibrations of Ti-O and Ti-O-Ti groups [34]. The effect of UV-Visible absorption spectrum was applied to investigate the effect of the percentage of chromium doped on the absorption properties of titanium dioxide. The results are shown in Figures 6. The band gaps (E_g) can be measured by Kubelka–Munk function as follows [34].

$$(\alpha hv)^{1/n} = E_D(hv - E_g) \qquad (3)$$

The energy gap (Eg) was calculated from the extrusion of the linear part of Figure 6 $(\alpha h\upsilon)^2$ in terms of hυ. According to Figure 6, the energy gap for pure titanium dioxide is 3.2 eV and for titanium dioxide with 2% chromium 2.79 eV, titanium dioxide with 8.5% chromium 2.5 eV and titanium dioxide with 15% chromium 2.7 eV is obtained. These results reveal that the TiO_2- Cr

composite could normally promote the visible light utilization efficiency and enhance the photo-catalytic activities.

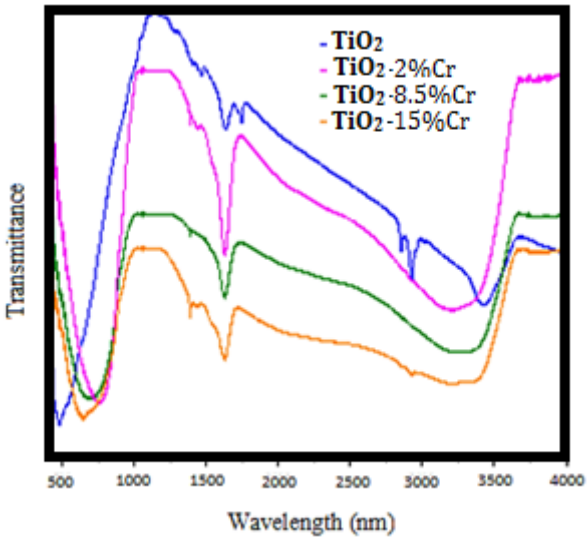

Figure 5: FT-IR spectrum

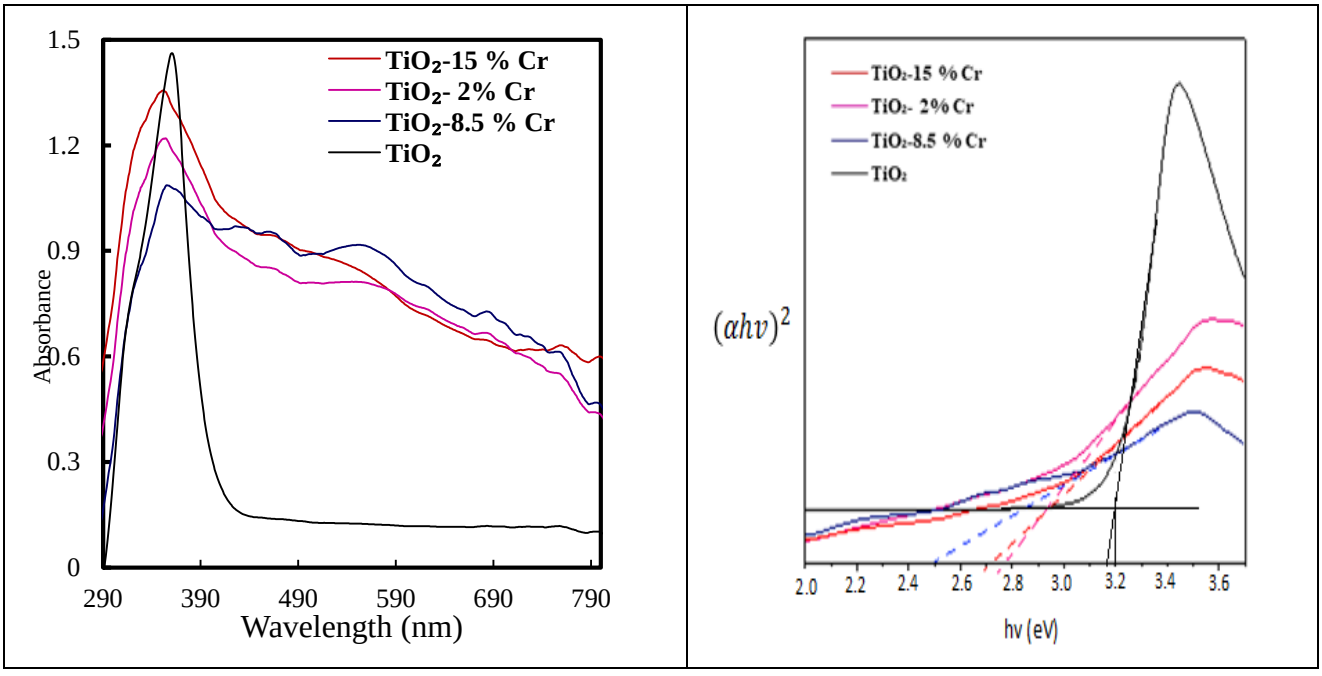

Figure 6: UV-Vis diffuse reflectance spectra of the samples and plots of $(\alpha hv)^2$ versus energy (hv) for TiO_2, Cr (%2)-TiO_2, Cr (%8.5)-TiO_2, and Cr (%15)-TiO_2

Physicochemical Characteristics Of WCO

The characteristics of acid number, soaping index, average molecular weight, density, and free fatty acid of WCO are presented in Table 1.

Free fatty acids are the result of the breakdown of triglycerides in the oil, which is higher in this type of oil due to the repeated use of waste oil. The higher the amount of free fatty acids, the greater the level of damage to the oil will be. In the transesterification process for biodiesel

production, the amount of free fatty acids should be less than % 0.5 to prevent saponification and stop the efficiency of biodiesel from reducing [35]. Therefore, in waste oils with high levels of free fatty acids, the esterification process is carried out in the initial step.

Table 1: Specifications of WCO

Value	Characteristic
8.14 mg $KOH.g^{-1}$	Acid number
180.01 mg $KOH.g^{-1}$	Soap Index
978.7 $g.mol^{-1}$	Molecular Weight
0.93 $g.cm^{-3}$	Density
4.09 %	Free fatty acid

Response Surface Analysis

In this study, a photocatalyst was used to reduce free fatty acids in the esterification step. In order to optimize the conditions at this stage, Design-Expert software and Box-Behnken design (BBD) were used. What follows pertains to the factors affecting the efficiency of photocatalyst in the first step of biodiesel production. The relationship between the three parameters of photocatalyst type, irradiation time, and methanol to oil ratio with fatty acid conversion percentage was investigated.

Table 2: Model summary statistics of FFAs conversion

Source	Std. Dev.	R-Squared	Adjusted R-Squared	Predicted R-Squared	PRESS	
Linear	3.50	0.8996	0.8765	0.8002	317.65	Suggested
2FI	3.03	0.9422	0.9076	0.7458	404.14	
Quadratic	3.29	0.9522	0.8908	0.3879	972.98	
Cubic	2.05	0.9894	0.9578		+	Aliased

As can be seen from Table 2, the linear model is proposed, in which the coefficient of explanation: 0.8966, adapted: 0.8765 and the predicted amount: 0.8002, the standard deviation of this model is 3.50 and the amount of PRESS is 317.65. The response level method was used for the model; the results of the analysis of variance for the dependent variable are summarized in Table 3.

Table 3: Summary of statistical results for linear equation

Std. Dev.	3.50	**R-Squared**	0.8996
Mean	50.95	**Adj R-Squared**	0.8765
C.V. %	6.88	**Pred R-Squared**	0.8002
PRESS	317.65	**Adeq Precision**	21.083
-2 Log Likelihood	86.31	**BIC**	97.64
		AICc	97.64

As indicated in Table 3 the value of R-Squared is 0.8996, indicating a good fit of the model with the original sample. As for the value of Adeq precision, which indicates the signal-to-noise ratio, if it is greater than 4, it is desirable and acceptable. In this model, this value is equal to 21.083, which is desirable. The value of the predicted explanation coefficient is 0.865, which is different from the value of the modified explanation coefficient that is 0.8002 less than 0.2, which is acceptable. Accordingly, it can be mentioned that the selected model is appropriate [36].

Three-dimensional and contour diagrams have been used to study the effects of interaction between independent parameters on the desired response. Figures 7a, 7b, and 7c show the contour line diagram and the three-dimensional diagram of the percentage of fatty acid conversion according to the interaction of the parameters and in the linear model.

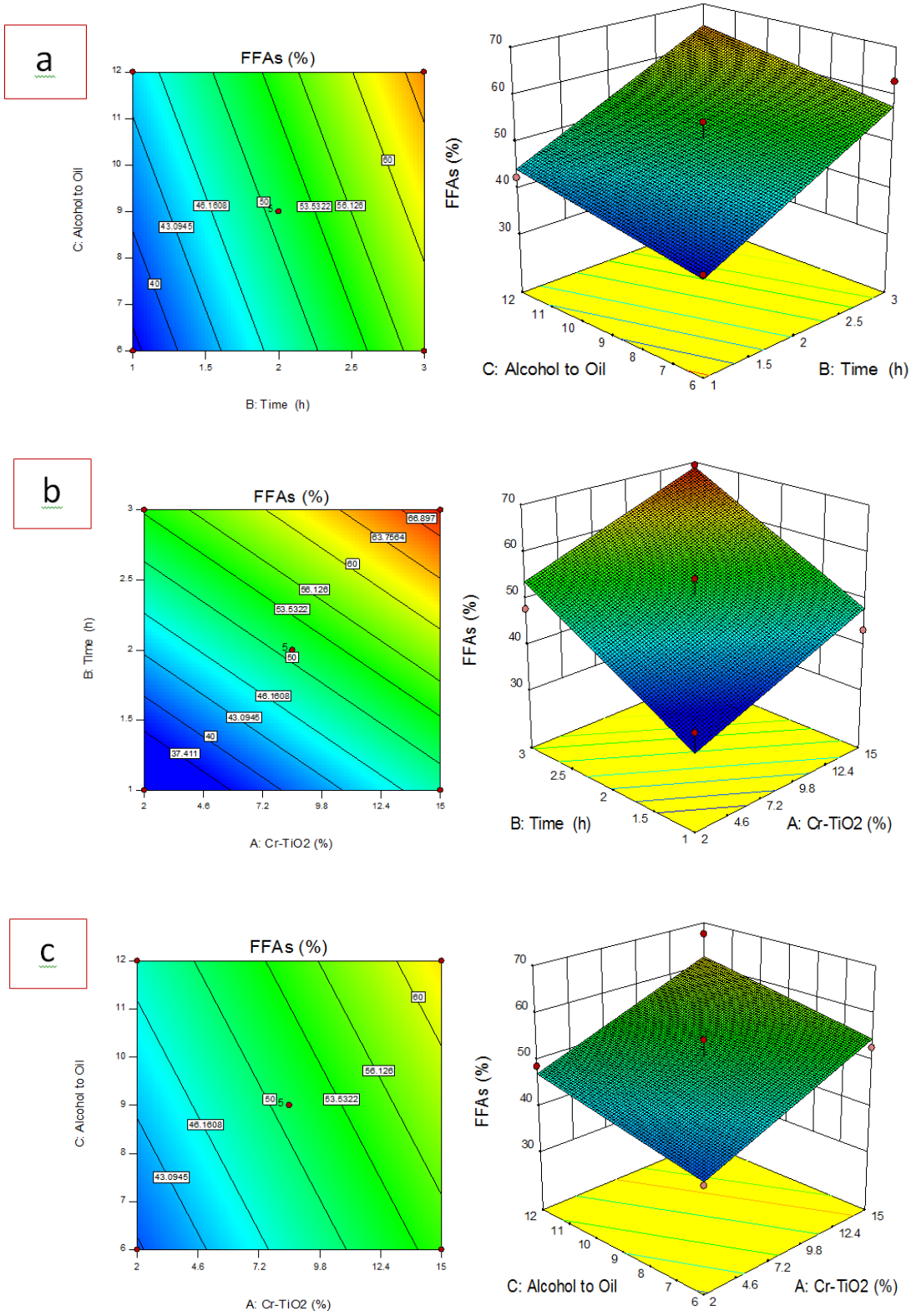

Figure 7: [a] Response surface graphs and contour plots of FFAs conversion, and the effect of molar ratio methanol to WCO and irradiation time. [b] the effect of irradiation time and photocatalyst type. [c] the effect of photocatalyst type and of molar ratio methanol to WCO

Figures 7a, b, and c show the three-dimensional diagram and contour of the response surface for the FFAs conversion to the photocatalyst type and the irradiation time in the photo-esterification step. It can be seen the conversion efficiency is observed with increasing time of increasing the efficiency with high slope. This increasing trend is also observed with increasing the percent of chromium in the TiO_2 structure so that the highest efficiency is seen in the presence of Cr (15%)-TiO_2 photocatalyst during 3 h of visible irradiation. Also, by the increase of the irradiation time and the ratio of alcohol to oil increases the conversion efficiency. Increasing the molar ratio of methanol to oil with a gentler slope has increased the efficiency and the effect of irradiation time is significant.

In Figure 7c, the shape of the interaction between the type of photocatalyst and the ratio of methanol to oil on the FFAs conversion is shown. By increasing both parameters, the conversion efficiency has increased. According to the software forecast, the reaction efficiency using TiO_2 photocatalyst is Cr (%15) and with the molar ratio of 12:1 methanol to WCO, it reaches its maximum value (67.4%).

Alkali Catalyzed Transesterification of WCO

In the following, we have examined the photo-esterification step using visible light irradiation on the efficiency of biodiesel. In the first step, photo-esterification was performed to reduce FFAs in WCO. In the second step, transesterification was used to produce biodiesel with obtained WCO in the previous step. Optimal test conditions obtained to reduce FFAs with Design-Expert software: pure TiO_2, Cr (%2)-TiO_2, and Cr (%8.5) -TiO_2 molar ratio of methanol to WCO;12 to 1, visible irradiation time; 3 h and for Cr (%15)-TiO_2 molar ratio of alcohol to WCO was 10.7 to 1 and irradiation time was 2 h and 56 min. In order to prepare these samples for the transesterification step, water and methanol were removed by Verma method [32]. A sample was examined as a control without photo-esterification step. The results are demonstrated in Figure 8.

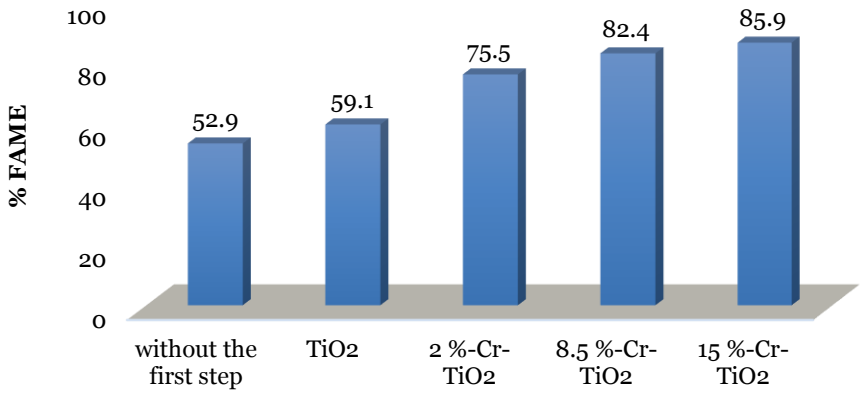

Figure 8: Biodiesel production using different conditions in the photo-esterification step

By performing the first step in the presence of visible light irradiation with Cr-TiO_2 photocatalysts, an efficiency of biodiesel production of 75.5%-85.9% was observed. In this experiment, it was observed that in the presence of TiO_2 photocatalyst, a 10% increase in efficiency could be observed compared with the sample without photocatalyst. Due to the energy

gap of TiO_2, which makes the creation of electron-holes with visible light impossible, the acidity of the surface TiO_2 and its high surface for the shape of its sheet can be the reason for the catalytic effect of TiO_2; this has been effective in reaction efficiency. It was observed that with increasing the percent of chromium in the structure of TiO_2, the efficiency increased, suggesting the positive effect of chromium content on the structure of TiO_2 to improve the conversion percentage of free fatty acids in the photo-esterification step. It should be noted that the transesterification conditions were the same for all samples.

Despite the high percentage of chromium on the TiO_2 structure with the collision of energy photons on the photocatalyst surface and the higher possibility of electron separation, this can improve the efficiency of reduced free fatty acids and affect the efficiency of biodiesel in the second stage.

Reusability of Catalyst

Photocatalyst recycling was tested in up to five steps. The results are shown in Figure 9.

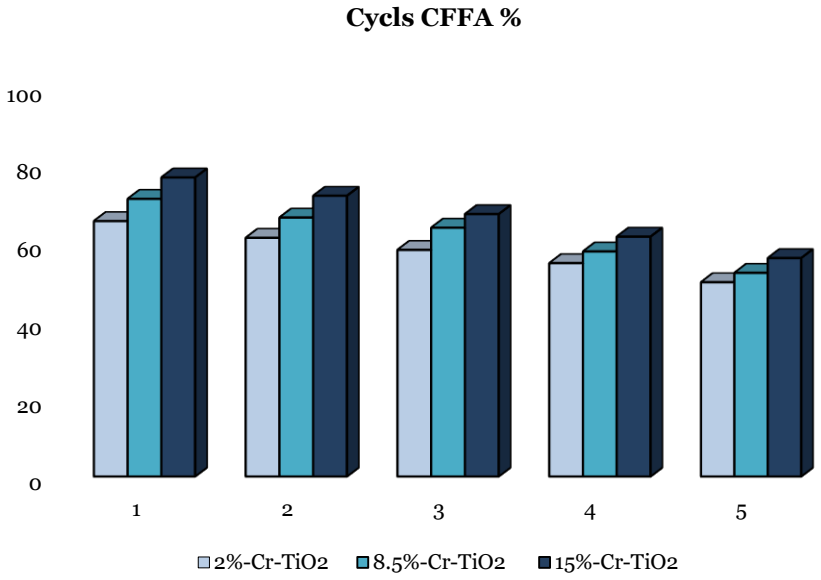

Figure 9: FFA conversion in five cycles of photocatalyst reusability

In Figure 9, the FFA conversion of the first cycle in the presence of photocatalysts for Cr (%2)-TiO_2, Cr (%8.5)-TiO_2, and Cr (%15)-TiO_2 were 65.6%, 71.3%, and 76.8%, respectively. After five cycles, the conversion rate was 49.9%, 52.3%, and 56.1% for the catalysts by visible light irradiation for 3 hours, respectively. The stability of catalysts indicates their suitable stability chemical. The highest reduction was related to Cr (%15)-TiO_2, which is due to the rugged surface of this catalyst compared with the two catalysts with Cr (2%) and Cr (%8.5). The FESEM images confirm differences in catalysts surfaces with different percent of chromium in the structures.

The unchanged catalytic activity of photocatalysts even after five cycles shows that there is a tiny reduction in catalyst mass due to decomposition and mass loss of chromium due to washing in the reaction mixture.

Kinetics of the Photo-Esterification Step

Mengli *et al.* method was used for kinetic study [26]. To study the kinetics of the Cr(%x)-TiO_2 photosynthesis reaction, an experimental study was performed (under conditions of Cr (%15)-TiO_2 photocatalyst, the molar ratio of alcohol to WCO (10.7:1)). The kinetic equation can be expressed as follows:

$$RCOOH + CH_3OH \longrightarrow RCOOCH_3$$

The conversion rate equation of FFA and methanol is expressed as follows:

$$-\frac{dC_A}{dt} = k\, C_A^a C_B^b \quad (4)$$

Which is considered in the equation $C_A = C_{A_0}(1 - X_A)$ and $C_B = C_{B_0}(1 - X_B)$, the concentrations of free fatty acids and methanol are at time t, respectively. C_{A_0} and C_{B_0} signify the initial concentrations of free fatty acids and methanol; a and b are the reaction order of free fatty acids and methanol; k represents the reaction rate constant; and X is the conversion of free fatty acids in the photo-esterification reaction. Due to the high concentration of methanol used, we consider the changes in methanol concentration to be constant. Therefore, it can be considered as a constant. If we consider that:

$$k' = k\, C_B^b \quad (5)$$

$$-\frac{dc_A}{dt} = k'\, c_A^a = -\frac{d[c_{A_0}(1-x)]}{dt} = \frac{dx}{dt} \quad (6)$$

$$\frac{dx}{dt} = \frac{k'\,[c_{A_0}(1-x)]^a}{c_{A_0}} \quad (7)$$

$$k'' = \frac{k'}{c_{A_0}} \quad (8)$$

$$\frac{dx}{dt} = k''\left[c_{A_0}(1-x)\right]^a \quad (9)$$

$$ln\frac{dx}{dt} = lnk'' + aln\left[c_{A_0}(1-x)\right] \quad (10)$$

Using this linear equation, the order of reaction and rate constant were calculated. a is the slope of the line indicating the order of the reaction and $ln\left[c_{A_0}(1-x)\right]$ is the y-intercept that is used to calculate the rate constant (Figure 10).

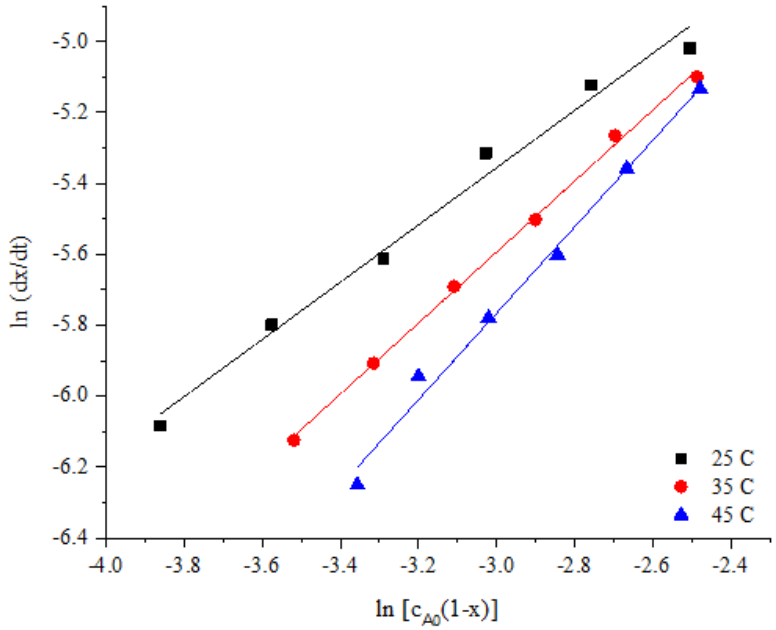

Figure 10: Diagram $ln\frac{dx}{dt}$ versus $ln\left[c_{A_0}(1-x)\right]$

Table 4 shows the rate constant, reaction order and correlation coefficient obtained. According to the obtained data, photocatalytic esterification by Cr-TiO_2 has been catalyzed with a reaction order of 1.008, which is approximately equal to one.

Table 4: Rate constant, reaction order, and correlation coefficient at different temperatures

Correlation coefficient	Reaction order (a)	Rate constant (k)	Temperatures (°C)
0.987	0.807	0.053	25
0.998	1.001	0.075	35
0.991	1.218	0.121	45

According to the rate constant and temperature, the activation energy is calculated by the Arrhenius equation:

$$nK = -\frac{E_a}{RT} + lnA \quad (11)$$

Given the linear regression coefficient, R^2 = 0.99079, the proposed reaction kinetics model is reasonable, and the activation energy required for the Cr-TiO_2 photocatalyst for WCO photosynthesis is 31.36 kJ/mol. The results of kinetic parameters show that Cr-TiO_2 photocatalyst requires less energy for WCO esterification and can be performed under mild conditions.

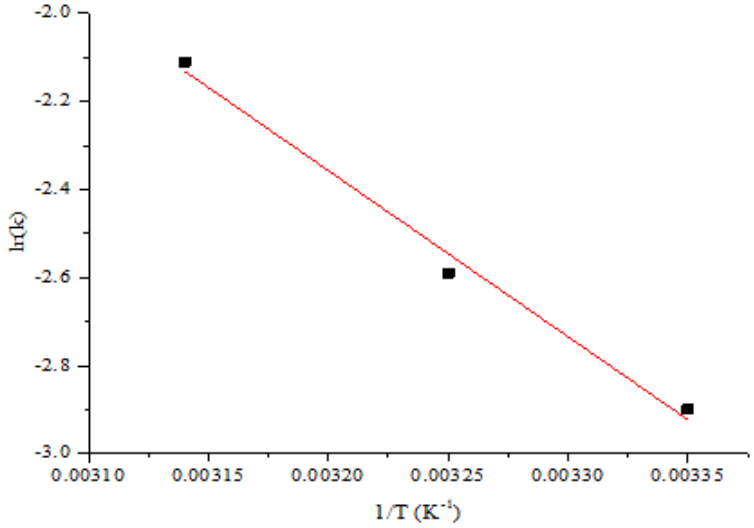

Figure 11: Arrhenius equation curve

Mechanism of the Photo-Esterification Step

The mechanism of the photocatalytic reaction is based on the generation of electron-hole pairs and their function in the reaction as follows: The impact of light with sufficient energy leads to the transfer of electrons from the TiO_2 capacitance band to the TiO_2 conduction band and the formation of holes in the TiO_2 capacitance band. Electrons are transferred to the conduction band and the holes formed in the capacitance band can react with the adsorbed species on the photocatalyst surface. According to the DRS curve, the energy gap for pure TiO_2 is 3.2 eV and for TiO_2 with %2 Cr is 2.79 eV; for TiO_2 with %8.5 Cr is 2.5 eV and TiO_2 with %15 Cr is obtained 2.7 eV. Obviously, doped Cr can significantly improve the absorption in the visible light region of TiO_2.
After irradiation, electrons are excited from the TiO_2 capacitance band and transferred to its conduction band, forming a hole in the capacitance band. As suggested by Senthil *et al.* [37], the overall reaction uses the pore oxidation energy directly and reacts with the adsorbed H_2O and OH on the surface to form a hydroxyl radical with strong oxidation properties. The reaction in the adsorption step follows the following steps (Scheme 1).

Characterization of WCO Biodiesel

Gas chromatography was used to determine the weight percentage of methyl esters in the samples (percentage of transesterification reaction conversion). This device is equipped with an FID detector and biodiesel column made by the Varian Company. The GC column used is polar type (0.30 mm x 0.32 mm) with CP9080 model and with static phase thickness of 0.25 mm. The gas chromatograph is of the CP3800 type. Fuel analysis was performed using EN 14103 standard and samples were performed with an internal standard of methyl heptadecanoate and N-heptane solvent. Helium is used as a carrier gas. Biodiesel samples were identified after preparation and injection into the

GC. Vegetable fats and oils are plant-derived lipids that are composed of triglycerides and are a mixture of fatty acids with carbon chains of different lengths as well as varying degrees of unsaturated carbon bonds. Some of the fatty acids commonly found in vegetable oils include: lauric (12:0), myristic (14:0), palmitic (16:0), palmitoleic (16:1), stearic (18:0), oleic (18:1), linoleic (18:2), linolenic (18:3), and so on. The two most common saturated fatty acids in vegetable oils are palmitic (16:0) and stearic (18:0). In addition, vegetable oils usually contain free fatty acids, water, sterols, phospholipids, odors, and other impurities. One of the most important properties of vegetable oils is the composition of fatty acids. The oil used in this study was waste cooking oil used from a set of vegetable oils and has no specific source. The results showed that it contained different types of fatty methyl esters (Table 5).

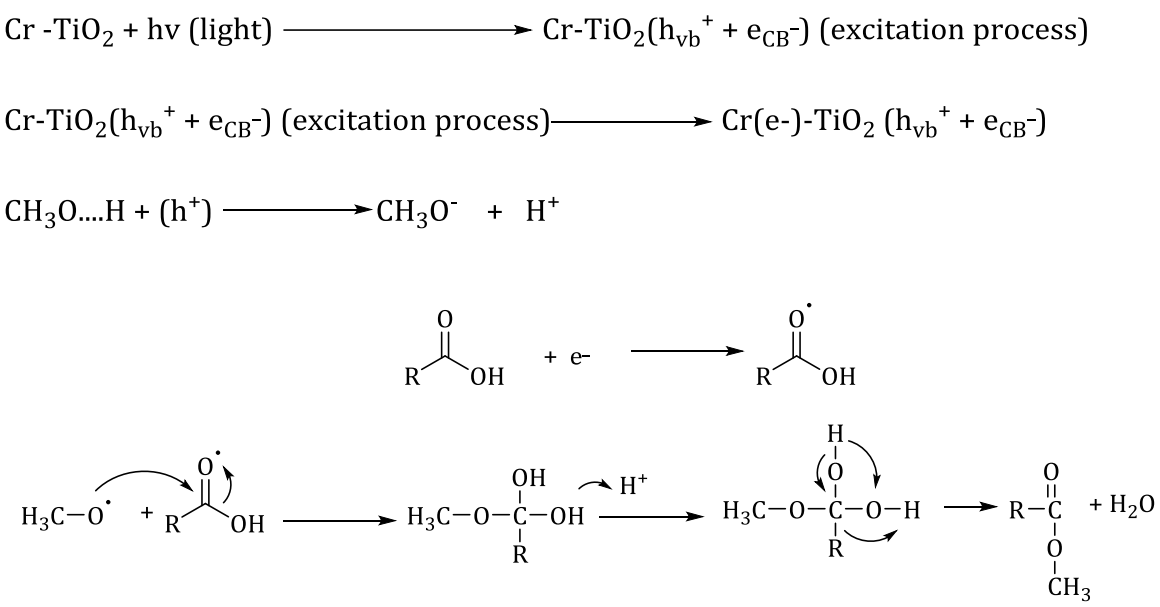

Scheme 1: Mechanism of the Photo-Esterification Step

Composition of fatty acids in WCO by GC is as follows: Palmitic acid %19.55, stearic acid %4.17, oleic acid %32.06, linoleic acid %31.75, linolenic acid %3.41, erucic acid 1.59%, neuronic acid %0.37, behenic acid %1.2, and other compounds were determined to be %4.99. The predominant fatty acid is oleic acid with %32.06 and the lowest amount of these acids is related to neuronic acid with %0.37. It should also be noted that saturated fatty acids (stearic and palmitic) and unsaturated (linoleic and oleic) are present in the WCO sample. The proportion of unsaturated fatty acids is higher than that of saturated fatty acids. Biodiesel samples were identified after preparation and injection into the device. Fatty acid monoesters in biodiesel fuels (palmitic, stearic, oleic, linoleic, and linolenic) affect the thermophysical properties of the fuel. Produced biodiesel contains different types of methyl esters. The predominant methyl esters in biodiesel produced are: methyl palmitic, methyl stearic, methyl oleic, methyl linoleic, methyl linolenic, and methyl myristic. The characteristics of biodiesel based on ASTMD standards were investigated. From the purified biodiesel, tests of viscosity, density, flash point, pour and cloud point, and the acid value of the biodiesel were performed.

According to the results of Table 5, measurement of biodiesel fuel properties produced in the presence of this catalyst indicates compliance of biodiesel properties with ASTM standards. This

fuel has a high flash point, a high ignition point increases safety in storage and transportation. The pour point and the cloud point for biodiesel are obtained as -5 and 0, respectively. According to the obtained results, the generated biodiesel density was 0.89 $g.cm^{-3}$. Another important result for measuring the properties of biodiesel is measuring its viscosity. The viscosity of 4.1 $mm^2.s^{-1}$ biodiesel from waste oil was measured, which corresponded to the standard range. The acid value of the biodiesel sample obtained from the waste oil is 0.38 mg KOH g^{-1}.

The FTIR spectrum is refined for one sample of WCO and for two samples of biodiesel with visible irradiation step conditions and the other sample with UV radiation (with %7.5 by weight of catalyst relative to WCO, the molar ratio of WCO to methanol 1:12 and the reaction time of 3 hours) and the transesterification step (catalyst concentration of %1, reaction time of 2 hours and the molar ratio of WCO to methanol 1:6) are shown in Figure 12. The product of the transesterification process (biodiesel) is chemically similar to its precursor (WCO), so very small differences can be observed between the spectra. In the region of 1700-1800 cm^{-1}, there is evidence of vibrational tensile bonding C=O, which confirms the presence of saturated aliphatic esters, which are common in the biodiesel and refined oil spectrum [38]. Medium peaks in 1459 and 1361 cm^{-1} are the reason for the existence of CH_2 and CH_3 vibratory bonds. Peaks 1245, 1200, 1180, and 1020 cm^{-1} are related to the C-O-C tensile bond. A strong peak at 1460 cm^{-1} indicates the presence of CH_3 in the biodiesel sample. The peak in the region at 725 cm^{-1} is the reason for the vibrational bond -CH_2. Strong peaks at 2950 cm^{-1} and 2850 cm^{-1} correspond to tensile C-H. The peak in 3450 cm^{-1} belongs to the OH group in alcohol and water, which is present in the oil sample with a sharp peak [39, 40].

Table 5: Comparison of biodiesel properties produced according to ASTM D6751 standard

Characteristics/properties	Standard Test (ASTM)	Estimated values
Density ($g.cm^{-3}$)	D-4052	0.89
Viscosity ($mm^2.s^{-1}$)	D-445	4.1
Acid value (mg $KOH.g^{-1}$)	D 664	0.38
Flash point (°C)	D-93	147
Cloudy point (°C)	D-2500	0
pour point (°C)	D-97	-5

Conclusion

The use of photocatalysts and the photo-esterification step in increasing the efficiency of biodiesel production is a reasonable and appropriate method. Reusable photocatalysts can be a convenient and cost-effective option. The main purpose of this study was to develop suitable processes for the production of biodiesel from oils with a high percentage of free fatty acids. Another goal is to understand the relationship between the percentages of free fatty acids in the oil source and reduce it using light sources and photocatalysts and biodiesel production efficiency. Biodiesel production from WCO was investigated by a two-step process. In the first step, the free fatty acids in the WCO were esterified with methanol by a photocatalytic process using a Cr/TiO_2 semiconductor composite and irradiation of visible irradiation as the light source. The catalytic performance of Cr/TiO_2 under different conditions in the WCO esterification process was investigated. The characterization results confirmed the synthesis of photocatalysts with two-dimensional structure. FESEM and TEM characterization has shown that Cr nanoparticles are located on the surface of TiO_2 nanosheets and DRS confirm the reduction of TiO_2 energy gap with different percentages of Cr doped on its surface. Energy gap for pure titanium dioxide, 3.2 eV; titanium dioxide with %2 chromium, 2.79 eV, titanium dioxide with %8.5 chromium, 2.5 eV and titanium dioxide with %15 chromium 2.7 eV

were obtained. The amount of free fatty acid in the WCO sample was 4.09%. In the sample formed without the esterification step, due to the effect of the high free fatty acid content of the soap, the separation of the product was difficult, which reduced the yield; the biodiesel production efficiency was 52.9%.

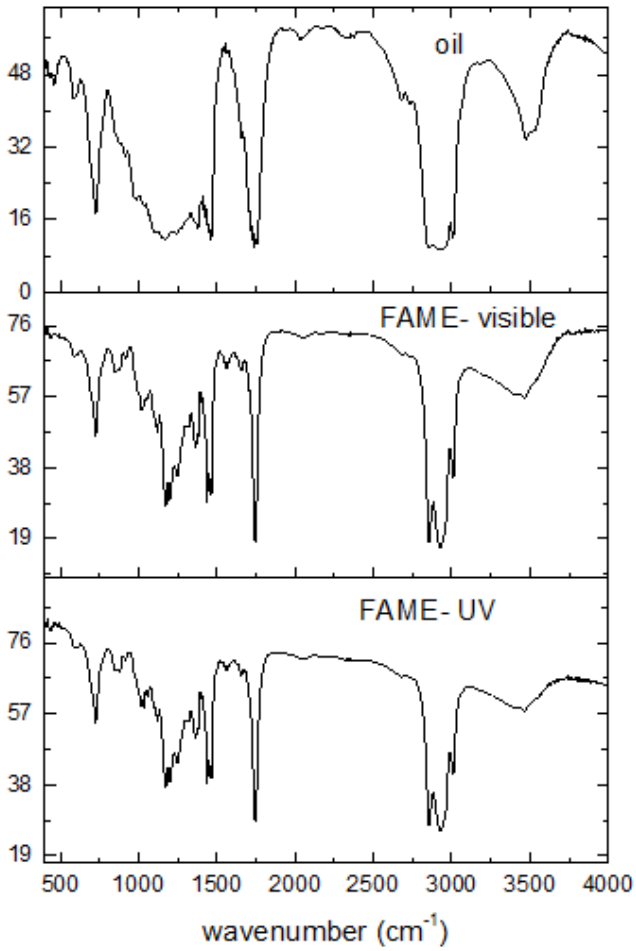

Figure 12: FTIR spectrum for a sample of refined WCO and for two samples of biodiesel with esterification step conditions by UV-Visible irradiation

While performing the esterification step in the presence of Cr-TiO_2 photocatalysts, the efficiency was 75.5%-85.9% with visible light irradiation. Photocatalytic recovery was investigated in five steps. After five experimental steps, with increasing the percentage of chromium on the structure of titanium dioxide, the surface of the structure is more rugged and with the recovery of photocatalysts, the probability of sediment penetration to active centers is higher and the efficiency naturally decreases in the later stages of catalyst use. The mechanism of photocatalytic reaction was investigated based on the production of electron-hole pairs. Exposure of light to sufficient energy leads to the transfer of electrons from the TiO_2 capacitance band to the TiO_2 conduction band and the formation of holes in the TiO_2 capacitance band. The electrons transferred to the conduction band and the holes formed in the capacitance band can react with the adsorbed species on the photocatalyst surface. Due to the DRS curve and the reduction of the energy gap for pure titanium dioxide relative to Cr-TiO_2, it is obvious that doped Cr has significantly improved the absorption in the visible light region of TiO_2.

To investigate the proposed mechanism of photon absorption by the Cr-TiO_2 photocatalyst, we relied mainly on TiO_2 sites, and the production of electrons induced by the e^- and the

h^+ and surface electrons in chromium atoms. The average density of synthesized biodiesel samples was 0.89 g/cm^3. The predominant methyl esters in biodiesel produced are: methyl palmitic, methyl stearic, methyl oleic, methyl linoleic, methyl linolenic, and methyl myristic.

Acknowledgements

This work was supported by the Iran National Science Foundation (INSF) of Iran (Grant No. 98028912). The authors acknowledge the financial supports from the Iran National Science Foundation extended to perform this research work.

Financial Interests

The authors declare they have no financial interests in this article.

Disclosure Statement

No potential conflict of interest was reported by the authors.

Funding

This work was supported by the Iran National Science Foundation (INSF) of IRAN (Grant No. 98028912).

Authors' Contributions

All authors contributed toward data analysis, drafting, and revising the paper and agreed to responsible for all the aspects of this work.

Conflict of Interest

The authors declare that they have no conflicts of interest in this article.

ORCID

Zahra Abbasi
https://orcid.org/0000-0001-9580-5423
Elisa I. Garcia-Lopez
https://orcid.org/0000-0002-1409-8921
Giuseppe Marci
https://orcid.org/0000-0003-2215-6543
Mehdi Ahmadi
https://orcid.org/0000-0002-9227-7562

References

[1]. Demirbas A., Biofuels sources, biofuel policy, biofuel economy and global biofuel projections, *Energy Conversion and Management*, 2008, **49**:2106 [Crossref], [Google Scholar], [Publisher]
[2]. Luque R., Lovett J.C., Datta B., Clancy J., Campelo J.M., Romero A.A., Biodiesel as feasible petrol fuel replacement: a multidisciplinary overview, *Energy & Environmental Science*, 2010, **3**:1706 [Crossref], [Google Scholar], [Publisher]
[3]. Schlick M., Hanna M., Schinstock J., Soybean and sunflower oil performance in a diesel engine, *Transactions of the ASAE*, 1988, **31**:1345 [Google Scholar], [Publisher]
[4]. Antolın G., Tinaut F., Briceno Y., Castano V., Perez C., Ramırez A., Optimisation of biodiesel production by sunflower oil transesterification, *Bioresource Technology*, 2002, **83**:111 [Crossref], [Google Scholar], [Publisher]
[5]. Fukuda H., Kondo A., Noda H., Biodiesel fuel production by transesterification of oils, *Journal of Bioscience And Bioengineering*, 2001, **92**:405 [Crossref], [Google Scholar], [Publisher]
[6]. Sharma Y., Singh B., Upadhyay S., Advancements in development and characterization of biodiesel: A review, *Fuel*, 2008, **87**:2355 [Crossref], [Google Scholar], [Publisher]
[7]. Granados M.L., Alba-Rubio A., Vila F., Alonso D.M., Mariscal R., Surface chemical promotion of Ca oxide catalysts in biodiesel production reaction by the addition of monoglycerides, diglycerides and glycerol, *Journal of Catalysis*, 2010, **276**:229 [Crossref], [Google Scholar], [Publisher]
[8]. Adel M.S., Ameri E., Individual and Simultaneous Isobutanol+ Nitromethane and 2-Ethylhexanitrate Influences on Diesel Fuel Property Indexes, *Chemical Methodologies*, 2021, **5**:381 [Crossref], [Publisher]

[9]. Poursadegh F., Aminkhani A., Evaluation of Chemical Compound of Thyme Essential Oil and Repelling and Lethality Effect of Thyme Plant Essential Oil on Rice Weevil, *Advanced Journal of Chemistry-Section B: Natural Products and Medical Chemistry*, 2023, **5**:51 [Crossref], [Publisher]
[10]. Korbag S., Korbag I., Trans-esterification of non-edible oil with a CaO-MgO heterogeneous catalyst to produce biodiesel, *Journal of Medicinal and Pharmaceutical Chemistry Research*, 2023, **5**:382 [Crossref], [Publisher]
[11]. Aliakbari M., Knowledge Management in Commercial Companies, *Eurasian Journal of Science and Technology*, 2022, **2**:268 [Crossref], [Publisher]
[12]. Abubaker M., Huo G., Shi J., Farah A., Zhang J., Gas Chromatography-Mass spectrum and Infra-Red spectral analysis of Fixed Oil from Sudanese Adansonia digitata Seeds, *Chemical Methodologies*, 2021, **5**:240 [Crossref], [Google Scholar], [Publisher]
[13]. Rahman M.A., Ferdous J., Hosen S., Hasan M., Parvin A., Shozib H.B., Hypercholesterolemia ameliorating effect of Bangladeshi high yield variety rice bran oil, *International Journal of Advanced Biological and Biomedical Research,* 2021, **9**:48 [Crossref], [Google Scholar], [Publisher]
[14]. Kazemi F., Zamani, H., Abedi, M.,Ebrahimi, M., Photodegradation of tramadol using α-Fe2O3 nanoparticles/12-tungstosilicic acid as an efficient photocatalyst in water sample employing box-behnken design, *Chemical Methodologies*, 2021, **5**:522 [Crossref], [Google Scholar], [Publisher]
[15]. Milani Fard A.M., Milani Fard M., Evaluation of Office Stones in Kidney Patients and How to form and Treat Them, *Eurasian Journal of Science and Technology*, 2022, **2**:111 [Crossref], [Publisher]
[16]. Mhaibes R. M., Arzehgar Z., Mirzaei Heydari M., Fatolahi L. ZnO Nanoparticles: A Highly Efficient and Recyclable Catalyst for Tandem Knoevenagel-Michael-Cyclocondensation Reaction, *Asian Journal of Green Chemistry*, 2023, **7**:1 [Crossref], [Google Scholar], [Publisher]
[17]. Jafari M., Investigating the Feasibility of Using Alumina-Zirconia Catalysts in Energy Production, *Progress in Chemical and Biochemical Research*, 2022, **5**:115 [Crossref], [Google Scholar], [Publisher]
[18]. Barzegar M., Zare A., Nano-$[Fe_3O_4@SiO_2@RNHMe_2][HSO_4]$: an effectual catalyst for the production of 1-amidoalkyl-2-naphthols, *Progress in Chemical and Biochemical Research*, 2022, **5**:68 [Crossref], [Publisher]
[19]. Ahmadlouydarab M., Javadi S., Adel Alijan Darab F., Evaluation of Thermal Stability of TiO_2 Applied on the Surface of a Ceramic Tile to Eliminate Methylene Blue Using Silica-based Doping Materials, *Advanced Journal of Chemistry, Section A*, 2023, **6**:352 [Crossref], [Google Scholar], [Publisher]
[20]. Heidaripour A., Salmani F., Barati T., Synthesis of Coral-Like ZnO Nanostructures with High and Wide Absorption Range, *Asian Journal of Green Chemistry*, 2023, **7**:140 [Crossref], [Google Scholar], [Publisher]
[21]. Samimi M., Challenges of Energy Carrier Consumption Management in Iran, *Eurasian Journal of Science and Technology*, 2022, **2**:242 [Crossref], [Publisher]
[22]. Mustafa Y.F., Chehardoli G., Habibzadeh S.، Arzehgar, Z., Electrochemical detection of sulfite in food samples. *Journal of Electrochemical Science and Engineering*, 2022, **12**:1061 [Google Scholar], [Publisher]
[23]. Arzehgar Z., Aydi A., Mirzaei Heydari M. Silver functionalized on hydroxyapatite-core-shell magnetic γ-Fe_2O_3: An enviromentaly and readily recyclable nanatalyst for the one-pot synthesis of 14*H*-dibenzo[a,j]xanthenes derivatives, *Asian Journal of Green Chemistry*, 2018, **2**:281 [Crossref], [Google Scholar], [Publisher]
[24]. Odogu Ankoro N., Ngouateu Lekene R.B., Ndi J.N., Kouotou D., Ngomo H.M., Ketcha J.M., Highly microporous activated carbons from Mangifera indica residues: Optimization of preparation conditions using response surface

methodology, *Asian Journal of Green Chemistry*, 2022, **6**:1 [Crossref], [Google Scholar], [Publisher]
[25]. Corro G., Pal U., Tellez N., Biodiesel production from Jatropha curcas crude oil using ZnO/SiO_2 photocatalyst for free fatty acids esterification, *Applied Catalysis B: Environmental*, 2013, **129**:39 [Crossref], [Google Scholar], [Publisher]
[26]. Guo M., Jiang W., Chen C., Qu S., Lu J., Yi W., Ding J., Process optimization of biodiesel production from waste cooking oil by esterification of free fatty acids using La^{3+}/ZnO-TiO_2 photocatalyst, *Energy Conversion and Management*, 2021, **229**:113745 [Crossref], [Google Scholar], [Publisher]
[27]. Park Y.M., Lee J.Y., Chung S.H., Park I.S., Lee S.Y., Kim D.K., Lee J.S., Lee K.Y., Esterification of used vegetable oils using the heterogeneous WO_3/ZrO_2 catalyst for production of biodiesel, *Bioresource Technology*, 2010, **101**:S59 [Crossref], [Google Scholar], [Publisher]
[28]. Mazzocchia C., Modica G., Kaddouri A., Nannicini R., Fatty acid methyl esters synthesis from triglycerides over heterogeneous catalysts in the presence of microwaves, *Comptes Rendus Chimie*, 2004, **7**:601 [Crossref], [Google Scholar], [Publisher]
[29]. Lertsathapornsuk V., Ruangying P., Pairintra R., Krisnangkura K., Continuous transethylation of vegetable oils by microwave irradiation. In *Proceedings of the 1st conference on energy network.* 2005, **2005** [Google Scholar],
[30]. Corro G., Sánchez N., Pal U., Cebada S., Fierro J.L.G., Solar-irradiation driven biodiesel production using Cr/SiO_2 photocatalyst exploiting cooperative interaction between Cr^{6+} and Cr^{3+} moieties, *Applied Catalysis B: Environmental*, 2017, **203**:43 [Crossref], [Google Scholar], [Publisher]
[31]. Abbasi Z., Ahmadi M., Process Optimization Photo-Esterification of Free Fatty Acids in Waste Cooking Oils under UV Irradiation via the RSM Method, *Chemical Methodologies*, 2023, **7**:799 [Crossref], [Publisher]
[32]. Verma P., Sharma M., Review of process parameters for biodiesel production from different feedstocks, *Renewable and Sustainable Energy Reviews*, 2016, **62**:1063 [Crossref], [Google Scholar], [Publisher]
[33]. Han X., Kuang Q., Jin M., Xie Z., Zheng L., Synthesis of titania nanosheets with a high percentage of exposed (001) facets and related photocatalytic properties, *Journal of the American Chemical Society*, 2009, **131**:3152 [Crossref], [Google Scholar], [Publisher]
[34]. Senthil R., Theerthagiri J., Selvi A., Madhavan J., Synthesis and characterization of low-cost g-C_3N_4/TiO_2 composite with enhanced photocatalytic performance under visible-light irradiation, *Optical Materials*, 2017, **64**:533 [Crossref], [Google Scholar], [Publisher]
[35]. Issariyakul T., Kulkarni M.G., Meher L.C., Dalai A.K., Bakhshi N.N., Biodiesel production from mixtures of canola oil and used cooking oil, *Chemical Engineering Journal*, 2008, **140**:77 [Crossref], [Google Scholar], [Publisher]
[36]. Ahmad M., Panda B.P., Optimization of red pigment production by Monascus purpureus MTCC 369 under solid-state fermentation using response surface methodology, *Songklanakarin Journal of Science and Technology*, 2014, **36**:439 [Google Scholar], [Publisher]
[37]. Senthil R., Theerthagiri J., Selvi A., Madhavan J., Synthesis and characterization of low-cost g-C_3N_4/TiO_2 composite with enhanced photocatalytic performance under visible-light irradiation, *Optical Materials*, 2017, **64**:533 [Crossref], [Google Scholar], [Publisher]
[38]. Kakati J., Gogoi T., Pakshirajan K., Production of biodiesel from Amari (Amoora Wallichii King) tree seeds using optimum process parameters and its characterization, *Energy Conversion and Management*, 2017, **135**:281 [Crossref], [Google Scholar], [Publisher]
[39]. Askari N., Farhadian M., Razmjou A., Simultaneous effects of pH, concentration, pressure on dye removal by a polyamide nanofilter membrane; optimization through response surface methodology, *Environmental Nanotechnology, Monitoring & Management*, 2018, **10**:223 [Crossref], [Google Scholar], [Publisher]

[40]. Eivari H.A., Ghasemi S.A., Tahmasbi H., Rostami S., Faraji S., Rasoulkhani R., Goedecker S., Amsler M., Two-dimensional hexagonal sheet of TiO_2, *Chemistry of Materials*, 2017, **29**:8594 [Crossref], [Google Scholar], [Publisher]

HOW TO CITE THIS ARTICLE
Zahra Abbasi, Elisa I. Garcia-Lopez, Giuseppe Marci, Mehdi Ahmadi. Biodiesel Production from Waste Cooking Oil Using Two-Dimensional Photocatalysts: Optimization of Process, Mechanism and Kinetics Study. *Chem. Methodol.*, 2024, 8(2) 133-153
DOI: https://doi.org/10.48309/CHEMM.2024.429360.1743
URL: https://www.chemmethod.com/article_189602.html